NJC

PAPER

Check for updates

Activation of chalcogen bonding in tetrathiafulvalene derivatives with Se/S differentiation†‡

Maxime Beau,[a] Ie-Rang Jeon, [ID] *[ab] Olivier Jeannin, [ID] [a] Thierry Guizouarn[a] and Marc Fourmigué [ID] *[a]

Activation of σ-holes on selenium atoms through the oxidation of the tetrathiafulvalene core in selenomethyl-substituted TTFs was evaluated in comparison with the less activatable thiomethyl moieties in 4,5-bis(methylseleno)-4′,5′-bis(methylthio)-tetrathiafulvalene **1**. Three charge-transfer complexes with TCNQ, TCNQF and TCNQF$_2$ were structurally characterized, with all of them showing a partial degree of charge transfer, ρ, in the range of $\pm 0.5 - \pm 0.6$, with alternating stacks of DDAADDAA patterns with TCNQ and DADADA patterns with TCNQF and TCNQF$_2$. No ChB interactions were identified in the latter two co-crystals, where MeSe and MeS- were disordered in 50 : 50 distribution, as also observed in the structure of neutral **1**. Alternatively, in the co-crystal with TCNQ, dissymmetric Se/S distribution (69 : 31) was associated with a strong Se···NC ChB interaction involving the majority Se atom. A similar preferential ChB interaction with Se was observed in the perchlorate salt (**1**)ClO$_4$, where the majority Se atom (71 : 29 Se/S distribution) interacts through Se···O ChB with the ClO$_4^-$ anion.

Introduction

The introduction of crystal engineering concepts[1,2] in the field of molecular conductors[3,4] has mainly relied on the substitution of the electroactive tetrathiafulvalene core with hydrogen bond (alcohols and amides) or halogen bond (iodine and bromine) donors.[5] These strategies are particularly successful with halogen bonding (XB) as the (partial) oxidation of TTF further activates XB donor groups (I and Br), even in solution,[6] enabling them to engage in strong, linear interactions with XB acceptors. This is observed in charge-transfer salts (with TCNQ and analogs),[7] as well as in cation radical salts with counterions such as Br$^-$,[8] ClO$_4^-$,[7c,9] and I$_3^-$,[10] all acting as Lewis bases. Besides XB, chalcogen bonding (ChB), which is based on σ-holes developed on a group 16 atom, has attracted interest in recent years,[11] initially toward anion recognition processes[12] and catalysis applications.[13] The demonstration that ChB can also play a significant role in crystal engineering strategies[14,15] prompted us and others to investigate its effects in molecular conductors,[16] radical anions[17] and neutral radical species.[18] In

our studies, we considered replacing the iodine atoms of iodinated TTFs by seleno- or telluroalkyl substituents. Thus, TTF oxidation is expected to selectively activate one of the two σ-holes in the chalcogen atom, which is located in the extension of the C$_{\text{TTF}}$–Ch(Alk) bond.[19] Our literature search showed that only few TTFs substituted with selenium atoms interacted with Lewis bases through ChB interactions,[20] and some of these examples are shown in Scheme 1a.

For example, the presence of the ethylenediseleno substituent in BEDS-TTF (also called BETS) favors the formation of Se···N ChB, although the overcrowding of the rigid six-membered ring limits the extent of this effect. Accordingly, we recently reported that the TTFs **A** and **B** (Scheme 1b) with geometrically well-disposed selenomethyl substituents were indeed able to engage in short linear Se···Br$^-$ ChB interactions in their cation radical salts with bromide.[21] Furthermore, a charge transfer complex of **A** with redox-modified TCNQF$_2$ as an electron acceptor was found to organize into original segregated stacks with metallic conductivity,[22] providing the first example of a TTF·TCNQ analog where ChB interactions play a dominant role in the structural organization of its salt.

Building on these positive results, we wanted to assess whether the ChB interaction in these systems was strong enough to dominate over a weaker competing interaction involving sulfur rather than selenium. For this purpose, we considered tetrathiafulvalene derivatives (Scheme 2) simultaneously bearing thioalkyl and selenoalkyl substituents to evaluate the possible S/Se differentiation through ChB in their salts. The corresponding BEDT-TTF analogs **C** and **D** were already described[23] but as reported for the BEDS-TTF
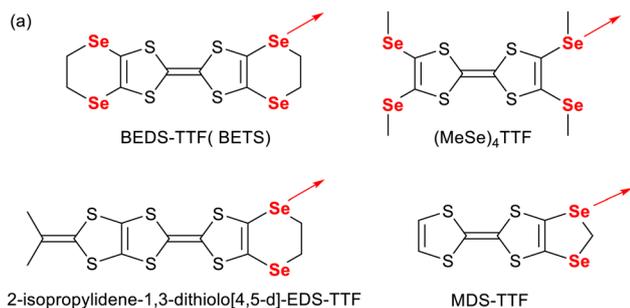
[a] *Univ. Rennes, CNRS, ISCR (Institut des Sciences Chimiques de Rennes), 35042 Rennes, France. E-mail: marc.fourmigue@univ-rennes.fr*

[b] *Univ. Bordeaux, CNRS, CRPP, UMR 5031, F-33600 Pessac, France. E-mail: ie-rang.jeon@u-bordeaux.fr*

† Dedicated to Professor Resnati, celebrating a career in fluorine and noncovalent chemistry on the occasion of his 70th birthday.

‡ Electronic supplementary information (ESI) available: Fig. S1–S5 and Tables S1–S3. CCDC 2445804–2445809. For ESI and crystallographic data in CIF or other electronic format see DOI: https://doi.org/10.1039/d5nj01745a

(a)

BEDS-TTF(BETS)   (MeSe)$_4$TTF

2-isopropylidene-1,3-dithiolo[4,5-d]-EDS-TTF   MDS-TTF

(b)

A   B

Scheme 1 Reported selenated TTFs engaged in ChB interactions in their salts. The red arrow shows the direction of the expected ChB interaction toward Lewis bases upon the activation of TTF through oxidation.

C   D

1   2
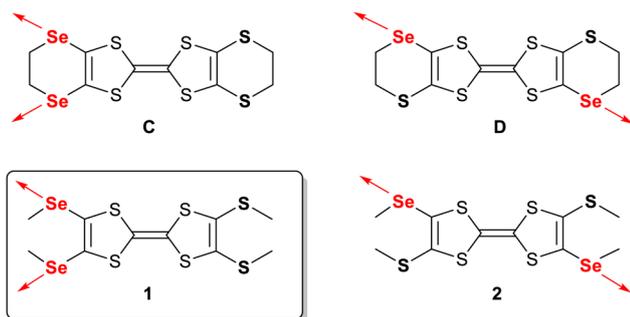
Scheme 2 Molecular structures of the target compounds. The red arrow shows the direction of the expected ChB interaction toward Lewis bases upon TTF activation through oxidation.

salts (Scheme 1a), the rigidity of the six-membered ring limits the accessibility of the σ-hole on the Se atom in engaging in ChB interaction; only one cation radical salt[24] was reported from **C** and none from **D**. Thiomethyl/selenomethyl-substituted TTFs **1** and **2** are unknown but offer more room and flexibility to allow the chalcogen atom to engage in ChB with acceptor molecules (such as TCNQ) or with anions (in cation radical salts).

Herein, we report here the first approach along these lines, concentrating on the non-centrosymmetric TTF derivative **1**. We describe its synthesis, X-ray crystal structure, charge-transfer complexes with TCNQ, TCNQF and TCNQF$_2$, and its salt with the ClO$_4^-$ anion.

Results and discussion

Synthesis, electrochemistry and crystal growth

TTF **1** was prepared (Scheme 3) through the phosphite coupling procedure of bis(selenomethyl) thione[25] **3** and cyanoethyl-protected dithiole-2-one[26] **4** to give **5**, as reported elsewhere.[27] Removal of the cyanoethyl protecting groups in **5** was
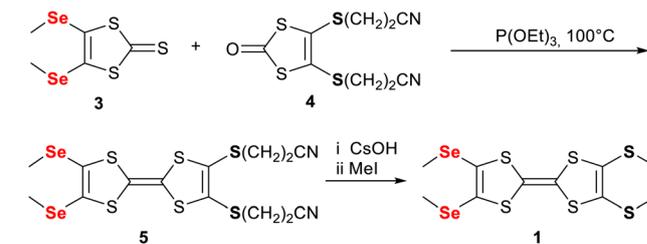
Scheme 3 Synthetic route to TTF **1**.

performed with CsOH, followed by alkylation with MeI to afford **1** in 83% yield. Cyclic voltammetry experiments (in CH$_2$Cl$_2$, 0.2 M Bu$_4$NPF$_6$ at 100 mV s^{-1}) showed the two successive reversible oxidation waves expected for this TTF derivative, which were observed at +0.47 and +0.82 V vs. SCE, and comparable to that found for (MeS)$_4$TTF (+0.48 and +0.80 V). Isolation of charge-transfer complexes or cations radical salts of **1** proved difficult given that the four chalcogenoalkyl groups endow **1** and its salts high solubility in many solvents.

Nevertheless, a charge-transfer complex of **1** with TCNQ was obtained by cooling a solution resulting from the diffusion of a solution of TCNQ in CH$_3$CN over a solution of **1** in CH$_2$Cl$_2$. After diffusion, no crystals appeared and cooling to −15 °C afforded crystals of a 1:1 phase, (**1**)·TCNQ. Similar experiments were conducted with TCNQF and TCNQF$_2$. Crystals of the 1:1 phase with TCNQF were obtained directly from the diffusion experiments, while crystals with TCNQF$_2$ were isolated after cooling at −15 °C. Besides, electrocrystallization experiments were conducted with different simple anions (Br$^-$, PF$_6^-$, and ClO$_4^-$) but systematically afforded highly soluble species. Performing electrocrystallization in EtOH with Et$_4$NClO$_4$ as the electrolyte allowed the isolation of high-quality crystals of the 1:1 phase formulated as (**1**)ClO$_4$.

Solid-state structures and properties

The neutral donor molecule **1** was found to crystallize in two different crystal forms, as needles and thin plates. The structure of the needle-like crystals was solved in the monoclinic system, space group $P2_1/c$, with one molecule disordered on an inversion center. Consequently, the central C$_6$S$_4$ TTF core is planar (Fig. 1a) and the thiomethyl and selenomethyl moieties are disordered with a 50:50 distribution. Alternatively, the structure of the plate-like crystals was solved in the monoclinic system, space group $P2_1/n$, with one molecule in the general position in the unit cell. As shown in Fig. 1b, it adopts a boat-like conformation through folding along the S···S hinges of the two dithiole rings by 23.5(4)° and 24.4(5)°. Moreover, the thiomethyl and selenomethyl moieties are still disordered, with a refined Se/S distribution close to 50:50 (52:48). The average intramolecular bond distances within the central TTF core are presented in Table 1, which were used to evaluate the degree of charge transfer in these compounds. In both structures, Se···Se intermolecular contacts were identified at 3.631(9) Å in **1**-flat and at 3.548(8) and 3.630(7) Å in **1**-boat, with the associated RR values of 0.93–0.96.[28] They lead to complex 3D interaction networks, as shown in Fig. S1 in the ESI.‡
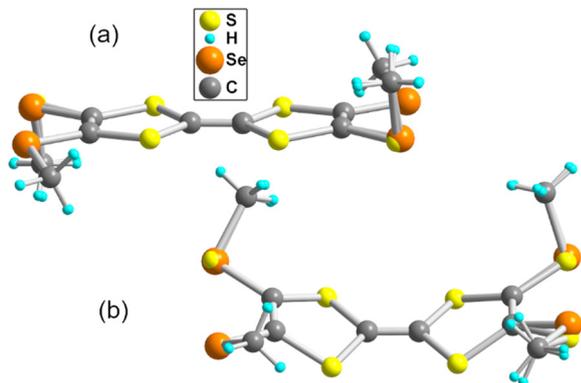
Fig. 1 Detailed molecular structure of **1** in the two polymorphs: (a) **1**-flat and (b) **1**-boat.

Table 1 Averaged bond distances (a–d in Å) in the TTF core of **1** and calculated charges, ρ_{TTF} from the linear extrapolation of the geometric parameter $\delta_{TTF} = (b - a)$ with $\rho_{TTF} = (\delta - \delta_{neutral})/(\delta_{cation} - \delta_{neutral})$, and ρ'_{TTF} from the formulae developed for BEDT-TTF, with the geometric parameter $\delta' = (b + c) - (a + d)$ (see text)

Compound	a	b	c	d	δ (Å)	δ' (Å)	ρ_{TTF}	ρ'_{TTF}
1-flat	1.319	1.759	1.750	1.349	0.440	0.8405	0	+0.07
1-boat	1.327	1.757	1.755	1.337	0.430	0.8487	0	+0.01
(**1**)·TCNQ	1.365	1.746	1.749	1.348	0.381	0.7830	+0.49/0.59	+0.50
(**1**)·TCNQF	1.356	1.743	1.745	1.341	0.387	0.7905	+0.43/0.53	+0.45
(**1**)·TCNQF$_2$	1.366	1.740	1.744	1.348	0.374	0.7702	+0.56/0.66	+0.60
(**1**)ClO$_4$	1.384	1.724	1.735	1.536	0.340	0.7197	+1	+0.98
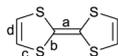
Comparison with the structures reported for the symmetric tetrakis(thiomethyl)- and tetrakis(selenomethyl)-tetrathiafulvalenes (MeS)$_4$TTF and (MeSe)$_4$TTF showed that (MeS)$_4$TTF is reported to crystallize into two different polymorphs,[29] with one of them isostructural with **1**-boat.[29a,b] Alternatively, (MeSe)$_4$TTF is reported to crystallize into two polymorphs,[30] both with a flat TTF core, where one has a short intermolecular Se···Se contact at 3.671(6) Å (RR = 0.97), and the other has two contacts at 3.639(5) and 3.619(5) Å (RR = 0.95). Altogether, these structures demonstrate the absence of highly directing interactions able to favor a specific supramolecular organization, with no clear differentiation between the S- and Se-containing moieties.

TCNQF$_n$ charge transfer complexes. Co-crystallization of **1** with TCNQ afforded a 1:1 phase crystallizing in the triclinic system, space group $P\bar{1}$, with both molecules in the general position in the unit cell. The central TTF core in **1** is essentially planar, with the folding angle along the S···S hinges of the two dithiole rings of 5.3(2)° and 1.8(2)°. The thiomethyl and selenomethyl moieties are also disordered, but with a 69:31 distribution, which is the first indication of preferential organization. The overall structural organization is formed by the stacking of inversion-centered homo-dimers, DDAADDAA, as shown in Fig. 2.

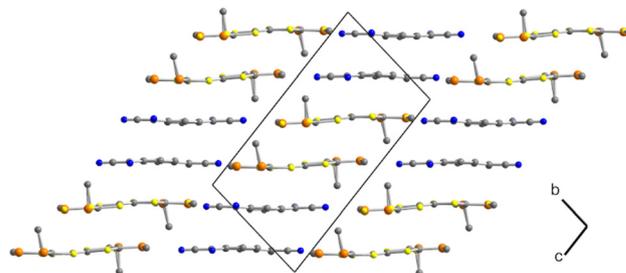The degree of charge transfer between the donor and acceptor was evaluated from the intramolecular bond lengths

Fig. 2 Projection view along a of the unit cell of (**1**)·TCNQ showing the DDAADDAA stacking motif.

within TTF derivative **1** (Table 1) as well as within the TCNQ molecule (Table 2), following correlations established earlier.[7a] The charge on **1** was determined by two methods, ρ_{TTF} from the linear extrapolation of the geometric parameter $\delta_{TTF} = (b - a)$ according to $\rho_{TTF} = (\delta - \delta_{neutral})/(\delta_{cation} - \delta_{neutral})$, and ρ'_{TTF} from the formula reported for BEDT-TTF, with the geometric parameter $\delta' = (b + c) - (a + d)$.[31] Both methods gave a TTF charge close to +0.5 in (**1**)·TCNQ. For the evaluation of the TCNQ charge, two formulas were also used, one based the linear extrapolation of the geometric parameter $\delta_{TCNQ} = c/(b + d)$ between the neutral and anionic compounds based on the equation $\rho_{TCNQ} = (\delta - \delta_{neutral})/(\delta_{anion} - \delta_{neutral})$,[32] and the other derived from the Kistenmacher formula[33] and developed for TCNQF$_n$ derivatives with the same δ_{TCNQ} parameter.[7a,34] They gave a TCNQ charge of −0.41/−0.45, confirming the partial charge transfer with (**1**)·TCNQ, which can be tentatively written as an alternating stack of mixed-valence homo-dimers, $[(\mathbf{1})_2]^+[(TCNQ)_2]^-[(\mathbf{1})_2]^+[(TCNQ)_2]^-$, with $\rho = \pm0.5$. In accordance with this charge state, the compound exhibits semiconducting behavior (Fig. S3 in ESI‡), with room temperature conductivity of $\sigma_{RT} = 1.1 \times 10^{-5}$ S cm^{-1} and an activation energy of 0.36 eV, indicating strong charge localization.

Perpendicular to the stacking axis, the molecules organize into layers in the $(b + c)$ plane, where they associate by ChB. As shown in Fig. 3, the very short Se···N≡C ChB interaction of 3.081 Å (RR = 0.81) involves mainly the selenium atom Se2A with occupation of 69%, while the minor component Se2B develops a much weaker interaction at 3.772 Å, well above the van der Waals contact distance (3.45 Å). Therefore, this structure offers the first illustration of the differentiation between S and Se atoms through ChB interaction, albeit it appears to be

Table 2 Average bond distances (a–d in Å) in the TCNQF$_n$ molecules and calculated charges, ρ_{TCNQ} from the linear extrapolation of the geometric parameter $\delta_{TCNQF_n} = c/(b + d)$ with $\rho_{TCNQF_n} = (\delta - \delta_{neutral})/(\delta_{anion} - \delta_{neutral})$, and ρ'_{TCNQF_n} from the formulae developed earlier (see text)

Compound	b	c	d	δ_{TCNQF_n}	ρ_{TCNQF_n}	ρ'_{TCNQF_n}
(**1**)·TCNQ	1.435	1.391	1.428	0.486	−0.45	−0.41
(**1**)·TCNQF	1.422	1.395	1.424	0.490	−0.62	−0.58
(**1**)·(TCNQF$_2$)	1.420	1.393	1.427	0.489	−0.65	−0.64
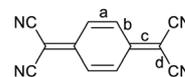
not strong enough to drive the preference for the Se atom to 100%.

Considering the first oxidation potential of **1** at +0.47 V *vs.* SCE and the reduction potential of TCNQ at +0.17 V, the negative but limited difference $\Delta E = E_{red} - E_{ox} = -0.30$ V can explain the partial charge transfer in this complex.[35] Replacing TCNQ with the stronger oxidant TCNQF (E_{red} = +0.28 V *vs.* SCE) or TCNQF$_2$ (E_{red} = +0.36 V *vs.* SCE) with the associated calculated values of ΔE of −0.19 and −0.11 V, respectively, should favor larger charge transfer between the donor and acceptor, and possibly enhance the ChB interactions through charge activation, as already demonstrated in halogen-bonded systems.[7a,36,37] (**1**)·TCNQF and (**1**)·TCNQF$_2$ were found to be isostructural, crystallizing in the triclinic system, space group $P\bar{1}$, with both molecules in the general position in the unit cell. The thiomethyl and seleno-methyl moieties in (**1**)·TCNQF are disordered, with a 55:45 distribution, the first indication of the absence of a predominant intermolecular interaction. The same MeSe/MeS disorder with a very similar distribution (54:46) was found in (**1**)·TCNQF$_2$. Concerning the acceptor molecules, the fluorine atom in TCNQF is disordered on four possible positions, with a 53:26:11:10 distribution, while in the TCNQF$_2$ compound, the fluorine atoms are also disordered with a 66:34 distribution. In the solid state, the molecules form alternating stacks DADADA, organized into layers in the (*a*,*c*) plane (Fig. 4). No characteristic ChB interactions can the found here, besides short S/Se···S/Se contacts involving only the outer MeS/MeSe substituents, between the donor molecules along the *b* axis. The partially positively charged S atoms of the TFF core are essentially surrounded by TCNQF or TCNQF$_2$ molecules (Fig. 4b). Evaluation of the degree of charge transfer in both salts (Tables 1 and 2) gave a value close to ±0.50 in (**1**)·TCNQF and a larger transfer in (**1**)·TCNQF$_2$ of around ±0.60.[38] The temperature dependence of the conductivity could not be determined for (**1**)·TCNQF$_2$ given that its crystals were too small but in (**1**)·TCNQF, it showed semiconducting behavior (Fig. S4 in ESI‡), with $\sigma_{RT} = 3 \times 10^{-5}$ S cm^{-1} and an activation energy of 0.35 eV, which is comparable to that determined for (**1**)·TCNQ and indicates the presence of strongly localized radical species.

Cation radical salt with ClO$_4^-$. The 1:1 cation radical salt of **1** obtained by electrocrystallization in EtOH crystallized in the triclinic system, space group $P\bar{1}$, with both the cation and ClO$_4^-$ anion in the general position in the unit cell. The thiomethyl and selenomethyl moieties are disordered, but with a 71:29 distribution, which is comparable to that observed in the TCNQ salt and most probably associated here with a structuring intermolecular interaction. Indeed, as shown in Fig. 5, one of the two main selenium atoms forms a short Se···O interaction
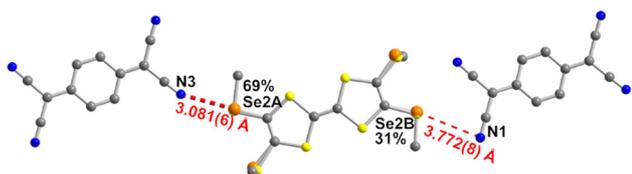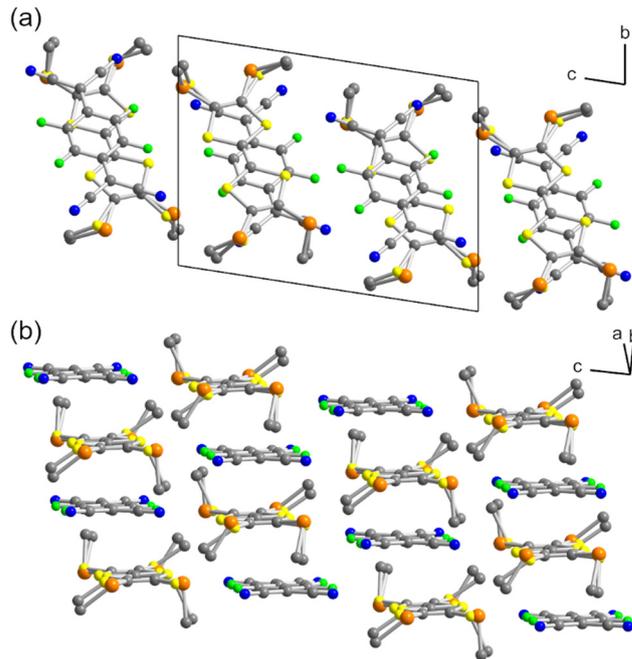

Fig. 4 Structure of (**1**)·TCNQF$_2$: (a) projection view of the unit cell along *a* and (b) details of one layer in the (*a*,*c*) plane with alternating DADA stacks. Hydrogen atoms were omitted for clarity.

(RR = 0.91) with the oxygen atom of the ClO$_4^-$ anion (also disordered), with the structural characteristics establishing unambiguously a strong ChB interaction. Furthermore, in contrast with the TCNQ charge transfer complex (*cf.* Fig. 3), the S/Se atoms on the other side of the molecule are not engaged in S/Se···O interactions. In the solid state, the cations organize into face-to-face diamagnetic dimers, as often encountered in ρ = +1 cation radical salts (Fig. S5, ESI‡).

Altogether, this work demonstrates that Se σ-hole activation in the extended C$_{TTF}$–Se bond can be strong enough to compete with similarly substituted sulfur atoms, but full ordering of the MeSe- and MeS-moieties with a 100% selective ChB on the Se atom is not achieved, at least in the two TCNQ and ClO$_4^-$ salts described here where ChB interactions occur. The origin of this
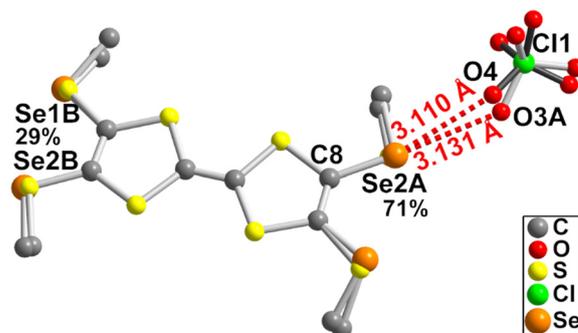

Fig. 3 Details of the ChB interaction in (**1**)·TCNQ.

Fig. 5 Details of the ChB interaction in (**1**)ClO$_4$, with the following structural characteristics: Se2A···O4 3.110(15) Å (RR = 0.91), C8–Se2A···O4 164.5(4)°; Se2A···O3A 3.131(18) Å (RR = 0.91), C8–Se2A···O3A 176.5(4)°.
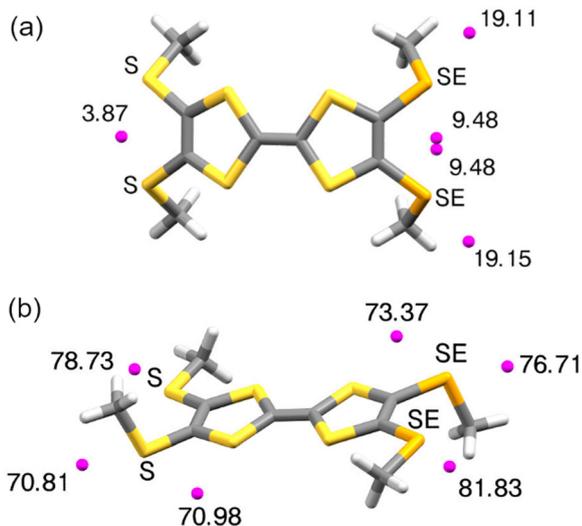
Fig. 6 Localization (pink dots) and maximum values of $V_{s,max}$ in the vicinity of the outer S and Se atoms in (a) **1** and (b) **1**$^{+\bullet}$ determined on geometry-optimized molecules (DFT, B3LYP/def2TZVP/D3).

behavior can be also found in the calculations of the electrostatic potential (ESP) surfaces (Fig. S6, ESI‡) of **1** and its cation radical **1**$^{+\bullet}$. As shown in Fig. 6a, the optimized geometry of neutral **1** gives a bent molecule (Fig. 1), with each dithiole ring containing one SMe (alternatively SeMe) group in the dithiole plane and one with the methyl group out-of-plane. In all cases (S *vs.* Se, in-plane *vs.* out-of-plane methyl group), the $V_{s,max}$ values are small, with the maximum values of +3.9 kcal mol^{-1} on the S side and +9.5 and +19.1 kcal mol^{-1} on the Se side, with the largest σ-hole in the extension of the C_{TTF}–Se bond. These values indicate effective S/Se differentiation in the neutral state. Upon oxidation to the cation radical state, these values strongly increase as anticipated, but the S/Se differentiation appears much more limited (Fig. 6b). Indeed, for the in-plane MeS/MeSe groups, the largest σ-hole in the extension of the C_{TTF}–S(Se) bond is 78.7 and 81.8 kcal mol^{-1}, while for the out-of-plane MeS/MeSe groups, the largest σ-hole in the extension of the C_{TTF}–S(Se) bond is 70.8 and 76.7 kcal mol^{-1}, respectively. These data offer a rationale for the absence of full S/Se ordering in the TCNQF$_n$ and ClO$_4^-$ salts reported herein, given that the σ-hole activation upon charge transfer also affects the S atoms of the SMe substituents to a large extent compared with the more polarizable Se atoms. Besides, the fact that the strongest σ-hole is found on the selenomethyl groups coplanar with the TTF core is also confirmed by the two experimental structures where this differentiation takes place, *i.e.*, the strong Se⋯N and Se⋯O ChB in the TCNQ and ClO$_4^-$ salts, respectively, indeed involving the coplanar selenomethyl groups (Fig. 3 and 5).

These observations contrast with similar experiments reported by Aakeroy *et al.* on halogen-bonded systems,[39] where the introduction of competition between iodine and bromine, for example in cocrystals involving 1-iodo-4-bromo-tetrafluoro-benzene or its biphenylene analog (Scheme 4), systematically led to complete I/Br disorder with 50 : 50 distribution in their co-crystals with symmetric bidentate XB acceptors such as
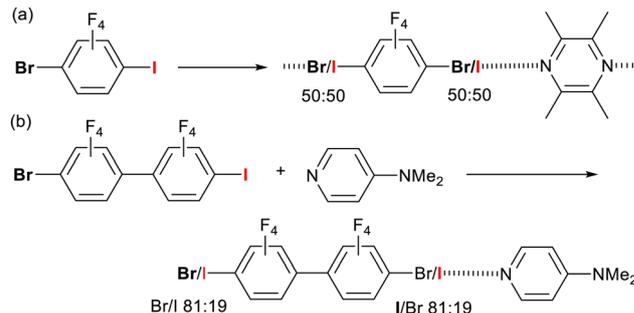
Scheme 4 Reported XB co-crystals with full I/Br disorder.[39]

tetramethylpyrazine. Moving to a single pyridine such as 4-dimethylaminopyridine promoted a preferential XB with iodine with a 81 : 19 I/Br distribution.

Conclusions

Activation of σ-holes on selenium atoms through the oxidation of the tetrathiafulvalene core in selenomethyl-substituted TTFs was evaluated from the comparison with the less activatable thiomethyl moieties in molecule **1** bearing both MeSe- and MeS-substituents. Three charge-transfer complexes with TCNQ, TCNQF and TCNQF$_2$ were structurally characterized, with all showing a partial degree of charge transfer, ρ, in the range ±0.5/±0.6, with alternating stacks of DDAADDAA patterns with TCNQ and DADADA with TCNQF and TCNQF$_2$. No ChB interactions were identified in the two latter co-crystals, where the MeSe and MeS are disordered in a 50 : 50 distribution, as observed also in the structure of neutral **1**. Conversely, in the co-crystal with TCNQ, the asymmetric Se/S distribution (69 : 31) is associated with the strong Se⋯NC ChB interaction of the main Se atom with the TCNQ cyano group. A similar preferential ChB interaction with Se was observed in the perchlorate salt (**1**)ClO$_4$, where the majority Se atoms (71 : 29 Se/S distribution) interact through Se⋯O ChB with the ClO$_4^-$ anion. A rationale for this limited differentiation effect can be found in the calculated electrostatic potential (ESP) surfaces on **1**$^{+\bullet}$, which show sizeable $V_{s,max}$ values on the outer S atoms, and larger ones only on the Se atoms belonging to selenomethyl groups fully coplanar with the TTF core. The comparison with reported halogen-bonded systems with Br/I competition and full disorder showed that the 70 : 30 distribution observed here in the two TCNQ and ClO$_4^-$ salts provides a clear signature of efficient differentiation between Se and S. Further work along these lines will focus on the other selenomethyl/thiomethyl-substituted TTF **2** mentioned in Scheme 2, where Se/S disorder can also compete with possible *Z/E* isomers.

Experimental

Chemicals and materials were obtained from commercial sources and used without further purification. All reactions were performed under an argon atmosphere. NMR spectra were recorded in CDCl$_3$ unless indicated otherwise. Chemical shifts are reported in ppm, ^{1}H NMR spectrum was referenced to

residual CHCl$_3$ (7.26 ppm) and ^{13}C NMR spectrum referenced to CHCl$_3$ (77.2 ppm). Melting points were measured on a Kofler hot-stage apparatus and are uncorrected.

Synthesis of 1

A solution of 2,3-bis(methylseleno)-6,7-bis(2-cyanoethyl)-tetrathiafulvalene[27] (760 mg, 1.36 mmol) in air-free dimethylformamide (15 mL) was cooled to 0 °C, and then a solution of CsOH·H$_2$O (660 mg, 3.93 mmol) in MeOH (5 mL) was added dropwise under an argon atmosphere. The red/orange solution was stirred for 90 min. Iodomethane (0.30 mL, 4.75 mmol) was added in one portion at 0 °C and stirring was maintained for 45 min. An orange precipitate appeared and was filtered. The filtrate was concentrated and the crude residue was solubilized in dichloromethane, washed with water and dried over MgSO$_4$. The solvent was evaporated under reduced pressure and the compound was separated by flash chromatography on a 24 g silica gel column. Elution with a gradient 0 → 20% of dichloromethane in petroleum ether gave compound **1** as a red powder (540 mg, 1.12 mmol, 83%). M.p. 98–100 °C. ^{1}H NMR (300 MHz, CDCl$_3$) δ 2.42 (s, 3H), 2.34 (s, 3H). ^{13}C NMR (300 MHz, CDCl$_3$) δ 127.72, 118.79, 19.34, 9.96.

Crystallography

Suitable crystals for X-ray diffraction single crystal experiments were selected and mounted on the goniometer head of a D8 Venture (Bruker-AXS) diffractometer equipped with a CMOS-PHOTON70 detector, using Mo-Kα radiation (λ = 0.71073 Å, multilayer monochromator). X-ray analyses were conducted each time on a single sample. Crystal structures were solved by dual-space algorithm using the SHELXT program,[40] and then refined with full-matrix least-squares methods based on F^2 (SHELXL program).[41] All non-hydrogen atoms were refined with anisotropic atomic displacement parameters. H atoms were finally included in their calculated positions and treated as riding on their parent atom with constrained thermal parameters. The crystallographic data from the X-ray data collection and structure refinements are given in Table S1 in ESI.‡

Resistivity measurements

The resistivity measurements were performed along the long axis of needle-shaped crystals of (**1**)·TCNQ and (**1**)·TCNQF. Gold wires were directly glued with silver paste on the single crystals. The measurements were conducted using a high-precision LCR meter (Keysight E4980A) at a frequency of 1000 Hz. The sample temperature was controlled using a physical property measurement system (PPMS, Quantum Design).

Theoretical calculations

Electrostatic potential calculations were carried out on the optimized geometry of the molecules (with density functional theory using the Gaussian 16, Revision C.01 software, the B3LYP functional and the def2TZVP basis set and D3 empirical dispersion correction for all atoms). GaussView 5.0.9 was used to generate the figures. The calculated ESP maps are presented in 0.001 e Bohr^{-3} isosurface (1 Bohr = 1 atomic unit (a.u.) = 0.529177249 Å).

Author contributions

I.-R. J. and M. F. formulated the project. M. B. synthesized and crystallized the compounds. O. J. collected and solved X-ray diffraction data, and performed theoretical calculations. T. G. performed electric measurements. M. F. wrote the paper, and all the authors contributed to revising it.

Conflicts of interest

There are no conflicts to declare.

Data availability

The data supporting this article have been included as part of the ESI.‡ CCDC 2445804–2445809 contain the supplementary crystallographic data for this paper.‡

Acknowledgements

References

1 G. R. Desiraju, J. J. Vittal and A. Ramanan, *Crystal Engineering, a Textbook*, World Scientific Publishing, Singapore, 2011.

2 L. Brammer, A. Peuronen and T. M. Roseveare, *Acta Crystallogr.*, 2023, **C79**, 204–216.

3 G. Saito and Y. Yoshida, *Top. Curr. Chem.*, 2012, **312**, 67–126.

4 P. Batail, *Chem. Rev.*, 2014, **104**, 4887–4890.

5 M. Fourmigué and P. Batail, *Chem. Rev.*, 2004, **104**, 5379–5418.

6 R. Oliveira, S. Groni, C. Fave, M. Branca, F. Mavré, D. Lorcy, M. Fourmigué and B. Schöllhorn, *Phys. Chem. Chem. Phys.*, 2016, **18**, 15867–15873.

7 (*a*) J. Lieffrig, O. Jeannin, A. Frąckowiak, I. Olejniczak, R. Świetlik, S. Dahaoui, E. Aubert, E. Espinosa, P. Auban-Senzier and M. Fourmigué, *Chem. – Eur. J.*, 2013, **19**, 14804–14813; (*b*) J. Lieffrig, O. Jeannin, T. Guizouarn, P. Auban-Senzier and M. Fourmigue, *Cryst. Growth Des.*, 2012, **12**, 4248–4257; (*c*) M. Iyoda, Y. Kuwatani, E. Ogura, K. Hara, H. Suzuki, T. Takano, K. Takeda, J. Takano, K. Ugawa, M. Yoshida, H. Matsuyama, H. Nishikawa, I. Ikemoto, T. Kato, N. Yoneyama, J. Nishijo, A. Miyazaki and T. Enoki, *Heterocycles*, 2001, **54**, 833–848; (*d*) J. Lieffrig, O. Jeannin, A. Vacher, D. Lorcy, P. Auban-Senzier and M. Fourmigué, *Acta Crystallogr.*, 2014, **B70**, 141–148.

8 (a) T. Imakubo, T. Shirahata, K. Hervé and L. Ouahab, *J. Mater. Chem.*, 2006, **16**, 162–173; (b) T. Imakubo, H. Sawa and R. Kato, *Synth. Met.*, 1995, **73**, 117–122; (c) O. Jeannin, E. Canadell, P. Auban-Senzier and M. Fourmigué, *Chem. Commun.*, 2016, **52**, 308–311.

9 (a) K.-S. Shin, M. Brezgunova, O. Jeannin, T. Roisnel, F. Camerel, P. Auban-Senzier and M. Fourmigué, *Cryst. Growth Des.*, 2011, **11**, 5337–5345; (b) K.-S. Shin, O. Jeannin, M. Brezgunova, S. Dahaoui, E. Aubert, E. Espinosa, P. Auban-Senzier, R. Swietlik, A. Frackowiak and M. Fourmigué, *Dalton Trans.*, 2014, **43**, 5280–5291.

10 (a) A. S. Batsanov, M. R. Bryce, A. Chesney, J. A. K. Howard, D. E. John, A. J. Moore, C. L. Wood, H. Gershtenman, J. Y. Becker, V. Y. Khodorkovsky, A. Ellern, J. Bernstein, I. F. Perepichka, V. Rotello, M. Gray and A. O. Cuello, *J. Mater. Chem.*, 2001, **11**, 2181–2191; (b) B. Domercq, T. Devic, M. Fourmigué, P. Auban-Senzier and E. Canadell, *J. Mater. Chem.*, 2001, **11**, 1570–1575.

11 (a) C. B. Aakeröy, D. L. Bryce, G. R. Desiraju, A. Frontera, A. C. Legon, F. Nicotra, K. Rissanen, S. Scheiner, G. Terraneo, P. Metrangolo and G. Resnati, *Pure Appl. Chem.*, 2019, **91**, 1889–1892; (b) R. Gleiter, G. Haberhauer, D. B. Werz, F. Rominger and C. Bleiholder, *Chem. Rev.*, 2018, **118**, 2010–2041.

12 (a) J. Y. C. Lim, I. Marques, A. L. Thompson, K. E. Christensen, V. Félix and P. D. Beer, *J. Am. Chem. Soc.*, 2017, **139**, 3122–3133; (b) G. E. Garret, E. I. Carrera, D. S. Seferos and M. S. Taylor, *Chem. Commun.*, 2016, **52**, 9881–9884; (c) S. Benz, M. Macchione, Q. Verolet, J. Mareda, N. Sakai and S. Matile, *J. Am. Chem. Soc.*, 2016, **138**, 9093–9096.

13 (a) S. Benz, J. Lopez-Andarias, J. Mareda, N. Sakai and S. Matile, *Angew. Chem., Int. Ed.*, 2017, **56**, 812–815; (b) P. Wonner, L. Vogel, M. Düser, L. Gomes, F. Kniep, B. Mallick, D. B. Werz and S. M. Huber, *Angew. Chem., Int. Ed.*, 2017, **56**, 12009–12012; (c) L. Vogel, P. Wonner and S. M. Huber, *Angew. Chem., Int. Ed.*, 2019, **58**, 1880–1891.

14 (a) P. Scilabra, G. Terraneo and G. Resnati, *Acc. Chem. Res.*, 2019, **52**, 1313–1324; (b) K. T. Mahmudov, M. N. Kopylovich, M. F. C. Guedes da Silva and A. J. L. Pombeiro, *Dalton Trans.*, 2017, **46**, 10121–10138; (c) M. Fourmigué and A. Dhaka, *Coord. Chem. Rev.*, 2020, **403**, 213084.

15 (a) N. Biot and D. Bonifazi, *Chem. – Eur. J.*, 2018, **24**, 5439–5443; (b) N. Biot, D. Romito and D. Bonifazi, *Cryst. Growth Des.*, 2021, **21**, 536–543; (c) P. C. Ho, P. Szydlowski, J. Sinclair, P. J. W. Elder, J. Kübel, C. Gendy, L. M. Lee, H. Jenkins, J. F. Britten, D. R. Morim and I. Vargas-Baca, *Nat. Commun.*, 2016, **7**, 11299.

16 (a) P. C. Ho, J. Z. Wang, F. Meloni and I. Vargas-Baca, *Coord. Chem. Rev.*, 2020, **422**, 213464; (b) M. Fourmigué and A. Dhaka, *Coord. Chem. Rev.*, 2020, **403**, 213084.

17 (a) T. Shimajiri, H.-P. Jacquot de Rouville, V. Heitz, T. Akutagawa, T. Fukushima, Y. Ishigaki and T. Suzuki, *Synlett*, 2023, 1978–1990; (b) T. Suzuki, C. Kabuto, Y. Yamashita, T. Mukai, T. Miyashi and G. Saito, *Bull. Chem. Soc. Jpn.*, 1988, 483–493.

18 (a) C. D. Bryan, A. W. Cordes, R. C. Haddon, R. G. Hicks, D. K. Kennepohl, C. D. MacKinnon, R. T. Oakley, T. T. M. Palstra and A. S. Perel, *J. Am. Chem. Soc.*, 1994, **116**, 1205–1210; (b) A. Mailman, S. M. Winter, X. Yu, C. M. Robertson, W. Yong, J. S. Tse, R. A. Secco, Z. Liu, P. A. Dube, J. A. K. Howard and R. T. Oakley, *J. Am. Chem. Soc.*, 2012, **134**, 9886–9889; (c) D. Tian, S. M. Winter, A. Mailman, J. W. L. Wong, W. Yong, H. Yamaguchi, Y. Jia, J. S. Tse, S. Desgreniers, R. A. Secco, S. R. Julian, C. Jin, M. Mito, Y. Ohishi and R. T. Oakley, *J. Am. Chem. Soc.*, 2015, **137**, 14136–14148.

19 A. Dhaka, I.-R. Jeon and M. Fourmigué, *Acc. Chem. Res.*, 2024, **57**, 362–374.

20 (a) M. Clemente-Leon, E. Coronado, J. R. Galan-Mascaros, C. Gimenez-Saiz, C. J. Gomez-Garcia, J. M. Fabre, G. A. Mousdis and G. C. Papavassiliou, *J. Solid State Chem.*, 2002, **168**, 616–625; (b) P. Wang, T. Inabe, C. Nakano, Y. Maruyama, H. Inokuchi, N. Iwasawa and G. Saito, *Bull. Chem. Soc. Jpn.*, 1989, **62**, 2252–2257; (c) M. Enomoto, A. Miyazaki and T. Enoki, *Bull. Chem. Soc. Jpn.*, 2001, **74**, 459–470; (d) K. Furuta, S. Kohno, T. Shirahata and Y. Misaki, *Eur. J. Inorg. Chem.*, 2014, 3982–3988; (e) K. Furuta, S. Kohno, T. Shirahata, K. Yamazaki, S. Hino and Y. Misaki, *Crystals*, 2012, **2**, 393.

21 M. Beau, O. Jeannin, M. Fourmigué, P. Auban-Senzier, F. Barrière and I.-R. Jeon, *CrystEngComm*, 2022, **24**, 7535–7539.

22 M. Beau, O. Jeannin, M. Fourmigué, P. Auban-Senzier, C. Pasquier, P. Alemany, E. Canadell and I.-R. Jeon, *CrystEngComm*, 2023, **25**, 3189–3197.

23 (a) L. Binet, J. M. Fabre and J. Becher, *Synthesis*, 1997, 26–28; (b) K. Takimiya, T. Jigami, M. Kawashima, M. Kodani, Y. Aso and T. Otsubo, *J. Org. Chem.*, 2002, **67**, 4218–4227.

24 S. Golhen, L. Ouahab, A. Lebeuze, M. Bouayed, P. Delhaes, Y. Kashimura, R. Kato, L. Binet and J.-M. Fabre, *J. Mater. Chem.*, 1999, **9**, 387–393.

25 M. R. Bryce, M. A. Coffin and W. Clegg, *J. Org. Chem.*, 1992, **57**, 1696–1699.

26 N. Svenstrup, K. M. Rasmussen, T. K. Hansen and J. Becher, *Synthesis*, 1994, 809–812.

27 L. Boudiba, A. K. Gouasmia and J. M. Fabre, *J. Soc. Alger. Chim.*, 2007, **17**, 77–85.

28 The reduction ratio (RR) is defined as the ratio of the experimental atom-atom distance over the van der Waals contact distance between these two atoms, based on van der Waals radii reported in.

29 (a) C. Katayama, M. Honda, H. Kumagai, J. Tanaka, G. Saito and H. Inokuchi, *Bull. Chem. Soc. Jpn.*, 1985, **58**, 2272–2278; (b) L. Wang, J.-P. Zhang and B. Zhang, *Acta Cryst.*, 2005, **E61**, o65; (c) H. Endres, *Z. Naturforsch.*, 1986, **B41**, 1351–1356.

30 (a) P. Wang, T. Inabe, C. Nakano, Y. Maruyama, H. Inokuchi, N. Iwasawa and G. Saito, *Bull. Chem. Soc. Jpn.*, 1989, **62**, 2252–2257; (b) C. Nakano, P. Wang, T. Mori, Y. Maruyama, H. Inokuchi, H. Yamochi and G. Saito, *Bull. Chem. Soc. Jpn.*, 1991, **64**, 3690–3693.

31 P. Guionneau, C. J. Kepert, G. Bravic, D. Chasseau, M. R. Truter, M. Kurmoo and P. Day, *Synth. Metals*, 1997, **86**, 1973–1974. The formula for BEDT-TTF salts reads as $\rho'_{TTF} = 6.347 - 7.463 \times \delta'_{TTF}$.

32 Based on reported crystal structures for neutral TCNQ and its radical anion, $\delta_{neutral}$ and δ_{anion} amount to 0.4756 and 0.4986 (see ref. 7a).

33 T. J. Kistenmacher, T. J. Emge, A. N. Bloch and D. O. Cowan, *Acta Crystallogr.*, 1982, **B38**, 1193–1199.

34 The formula for TCNQ salts reads as $\rho'_{TCNQ} = 19.833 - 41.667 \times \delta_{TCNQ}$.

35 (*a*) J. B. Torrance, J. E. Vazquez, J. J. Mayerle and V. Y. Lee, *Phys. Rev. Lett.*, 1981, **46**, 253–257; (*b*) G. Saito and J. P. Ferraris, *Bull. Chem. Soc. Jpn.*, 1980, **53**, 2141–2145.

36 (*a*) A. Frackowiak, I. Olejniczak, R. Swietlik, O. Jeannin and M. Fourmigué, *J. Phys. Chem. C*, 2016, **120**, 23740–23747; (*b*) A. Frąckowiak, R. Świetlik, L. Maulana, D. Liu, M. Dressel, O. Jeannin and M. Fourmigué, *J. Phys. Chem. C.*, 2020, **124**, 5552–5558; (*c*) A. Frąckowiak, R. Świetlik, I. Olejniczak, O. Jeannin and M. Fourmigué, *Spectrochim. Acta, Part A*, 2025, **329**, 125537.

37 (*a*) J. Lieffrig, O. Jeannin, T. Guizouarn, P. Auban-Senzier and M. Fourmigué, *Cryst. Growth Des.*, 2012, **12**, 4248–4257; (*b*) J. Lieffrig, O. Jeannin, A. Vacher, D. Lorcy, P. Auban-Senzier and M. Fourmigué, *Acta Crystallogr., Sect. B: Struct. Sci., Cryst. Eng. Mater.*, 2014, **B70**, 141–148.

38 The formulae for TCNQF and $TCNQF_2$ salts read as $\rho'_{TCNQF} = 27.79 - 57.87 \times \delta_{TCNQF}$ and $\rho'_{TCNQF_2} = 27.79 - 57.87 \times \delta_{TCNQF_2}$ (see ref. 7a).

39 C. B. Aakeröy, P. D. Chopade and J. Desper, *Cryst. Growth Des.*, 2013, **13**, 4145–4150.

40 G. M. Sheldrick, *Acta Cryst.*, 2015, **A71**, 3–8.

41 G. M. Sheldrick, *Acta Cryst.*, 2015, **C71**, 3–8.